Role of Ce in Manipulating the Photoluminescence of Tb doped Y₂Zr₂O₇

Yuming Wang, ^a Pragathi Darapaneni, ^a Orhan Kizilkaya, ^b James A. Dorman ^{a,*}

^a Cain Department of Chemical Engineering, Louisiana State University, Baton Rouge, Louisiana 70803, United States

^b Center for Advanced Microstructures and Devices, Louisiana State University, Baton Rouge, Louisiana 70806, United States

ABSTRACT Y₂Zr₂O₇ (YZO) is widely used as a host material for luminescent centers because of its high stability and the ability to accommodate anion defects. In this work, the effects of Ce and Tb doping on the photoluminescence (PL) properties of YZO nanoparticles (NPs) is studied in detail to correlate the emission intensity with the dopant concentration. Herein, a two-step synthesis method of co-precipitation and molten salt was employed to prepare the YZO:Tb, Ce NPs. The single doped YZO:Tb (2 mol%) NPs shows a strong Tb³⁺ emission. However, after co-doping with Ce ions, the Tb³⁺ emission is quenched instead of the expected sensitization. To identify the mechanism of quenching (oxidation state/local symmetry), X-ray absorption spectroscopy (XAS) and X-ray photoelectron spectroscopy (XPS) were performed. The Ce⁴⁺ ions were observed to drive further oxidation of Tb to a non-luminescent 4+ oxidation state. Alternatively, Eu³⁺ was employed to probe local symmetry changes upon Ce doping. The

asymmetry ratio of the magnetic and electronic transitions indicates the Ce dopant also pushes the system into a higher symmetry, resulting in two separate quenching mechanisms.

1. Introduction

The ability to control the oxygen vacancy concentration in A₂B₂O₇ nanoparticles (NPs) has been the research interest of several groups owing to the interrelationship between vacancy concentration and A-site symmetry. ¹⁻³ Specifically, rare earth (RE)-based binary metal oxides of the form RE₂B₂O₇ (RE = RE³⁺ and B = smaller quadrivalent cation, for example, Zr⁴⁺, Ti⁴⁺, Hf⁴⁺) have been used for wide-ranging applications such as oxide ion conductors, ⁴ catalysts, ⁵⁻⁶ pigments, ⁷ thermal barrier coatings, ⁸ and host materials for luminescence centers ⁹⁻¹² due to their excellent luminescence and oxygen storage properties. These compounds typically crystallize in a disordered fluorite structure when the ratio of ionic radii of RE and B sites is less than 1.46, under ambient conditions. ¹³⁻¹⁵ Further, the equivalent cationic sites (RE, B) gives rise to a random distribution of the oxygen vacancies and lowers the overall crystal symmetry. ¹⁶ Moreover, doping trace amounts of aliovalent ions in these crystals can control the concentration of these oxygen vacancies and manipulate the cation-oxygen bond strain, impacting the luminescent, photocatalytic, and electrical properties of the doped system. ¹⁷⁻²⁰

Among various RE-based metal oxides, the disordered $Y_2Zr_2O_7$ (YZO) fluorite crystal has been studied as a potential host material for luminescent ions (pairs) such as $Eu^{3+}, ^{21}$ $Dy^{3+}, ^{22}$ $Eu^{3+}, ^{23}$ and $Tb^{3+}, ^{24}$ With the inclusion of Tb^{3+} into the YZO host, a green emission centered at ~545 nm is reported due to the 5D_4 - 7F_5 transition. $^{25-27}$ Typically, the intensity of these Tb^{3+} emission peaks is enhanced via sensitization with other dopants, such as Ce^{3+} . In this regard, Ce^{3+} can act as a good sensitizer by facilitating energy transfer to Tb^{3+} ions $^{28-32}$, as reported in

Y₂Sn₂O₇:Ce³⁺, Tb³⁺ 3³, YPO₄:Ce³⁺, Tb³⁺ 3⁴, and LaPO₄:Ce³⁺, Tb³⁺ 3⁵. The sensitization of Tb³⁺ with Ce³⁺ is attributed to the strong Ce³⁺ 4*f*-5*d* absorption in UV region (250-350 nm) which couple with the intra *f-f* transitions of Tb. 36-37 Despite this, there are no reports available for Ce sensitization of Tb³⁺ in YZO host matrices. Therefore, this work aims to understanding the Ce³⁺-Tb³⁺ coupling mechanisms in A₂B₂O₇ hosts, with a specific focus on YZO, to enhance Tb³⁺ emission intensity and efficiency. 29, 33

In this work, a two-step co-precipitation/molten salt synthetic method was employed to prepare YZO:Tb, Ce and YZO:Eu³⁺, Ce NPs with varying RE (Tb, Eu, Ce) doping concentrations. A detailed structural characterization was performed using XRD, HRTEM, and Raman spectroscopy to affirm the homogeneous doping and crystalline phase (disordered fluorite) of the NPs. Furthermore, the effect of Ce doping on Tb luminescence intensity in the YZO host crystal was systematically studied using photoluminescence spectroscopy (PL) to elucidate the Ce-Tb energy transfer mechanism. Contrary to the expected sensitization of Tb luminescence with Ce, the Tb luminescence emission intensity was quenched after introducing trace amounts of Ce into the YZO:Tb system. While the XPS and XANES results indicate an oxidation of the luminescence center (Tb³⁺) to Tb⁴⁺ upon Ce doping, the changes in the local symmetry around the luminescence center were also investigated using another RE element, Eu³⁺, due to its symmetry-dependent luminescence. The intensity of ratio of electric (ED, ⁵D₀-⁷F₂ transition at 607 nm) to magnetic (MD, 5D_0 - 7F_1 transition at 590 nm) dipoles, referred to as the asymmetry ratio (R), has been applied to quantify the local crystal environment around the Eu³⁺ dopants.³⁸ The R value extracted from the Eu³⁺ luminescence after substitution in YZO host revealed local symmetry changes around the luminescent center (Tb³⁺/Eu³⁺) due to Ce doping. Combining the results of XPS, XANES, and PL, it can be concluded that the oxygen vacancy concentration is

inversely proportional to the Ce concentration, resulting in a high-local symmetry structure. While this work has direct implications in controlling the luminescence of nanophosphors via oxidation state and symmetry tuning, it can be extended to other host systems that require control over oxygen vacancies such as oxide ion conductors, photocatalysts, and semiconductors.³⁹⁻⁴¹

2. Experimental Section

2.1. Synthesis of Co-Doped Yttrium Zirconium Oxide (Y₂Zr₂O₇, YZO) NPs. YZO:Tb, Ce NPs were synthesized using a two-step co-precipitation/molten salt method. 42-43 In this work, three different Tb concentrations (2, 2.5, 12.5 mol%) with three different co-dopant (Ce) molar ratios (Tb:Ce = 1:5, 1:1, 5:1) were employed. For example, the YZO:Tb (2 mol%), Ce (2 mol%) was prepared by dissolving 7.68 mmol of yttrium(III) nitrate hexahydrate (Y(NO₃)₃·6H₂O, Alfa Aesar, 99.9%), 0.16 mmol of terbium(III) nitrate hexahydrate (Tb(NO₃)₃·6H₂O, Alfa Aesar, 99.99%), 0.16 mmol of cerium(III) nitrate hexahydrate (Ce(NO₃)₃H₂O, Strem Chemicals, 99.9%) and 8.0 mmol of zirconium dinitrate oxide hydrate (ZrO(NO₃)₂·xH₂O, Beantown Chemical, 99.9%) in 400 mL of deionized (DI) water under vigorous magnetic stirring. Next, 400 mL of ammonium hydroxide (NH₄OH, 28-30%, ACS grade) was added to the above solution dropwise and stirred for 2 h. The precipitate was filtered and washed with DI water several times until the pH of the solution was 7. After washing and filtering, the precipitate was dried overnight at 100 °C. The dried precipitate was then mixed and ground with a eutectic mixture of NaNO₃ (high purity grade, VWR Amresco, 99.0%) and KNO₃ (ACS grade, VWR Amresco) to form a homogeneous powder. The mixture was heated to 650 °C for 6 h with a heating rate of 10 °C/min. After cooling to room temperature, the resultant powder was washed several times with DI water and dried overnight at 100 °C to obtain co-doped YZO:Tb, Ce NPs. Similar synthetic

route was employed to prepare the YZO:Eu, Ce NPs with varying Eu and Ce doping concentrations.

- 2.2. Powder X-ray Diffraction (XRD). The crystal structure was studied by performing powder XRD using PANalytical X-ray diffractometer operating at 45 kV and 40 mA. The 2 θ radial scan was performed using Cu K α (λ =1.54 Å) radiation source from 5 to 70 $^{\circ}$ with a step size of 0.03 $^{\circ}$.
- 2.3. Raman Spectroscopy. Raman spectroscopy was performed with Renishaw inVia Reflex Raman Spectrometer. A 0.05 mW diode laser was used with an excitation wavelength of 532 nm, exposure time of 0.5 s, and spectral resolution of 1 cm⁻¹ in the measurements. The diameter of the focused laser spot on the sample at 50x magnification was approximately 5 μm. The spectra reported here are obtained after averaging the data from three scans.
- 2.4. Photoluminescence (PL) Spectroscopy. The photoluminescence and lifetime measurements were performed on an Edinburgh FLS1000 PL spectrometer equipped with a PMT detector and a 450 W ozone-free xenon arc lamp as light source. For PL measurements, the powder samples were placed into a quartz spectrophotometer cell (Starna Cells, Inc). The excitation and emission scans were collected with a bandwidth of 3 nm, dwell time of 0.5 s, and a step size of 1 nm in the range of 220-400 nm and 450-750 nm, respectively. The lifetime measurements were performed with a microsecond flash lamp (frequency: 25 kHz, 1-2 μs pulse) over the range of 10 ms with a 2 ms delay time, resulting in a 5 μs detector response (2000 channels). For all the measurements, a 250-380 nm excitation filter was used to reduce the baseline noise due to the lamp. The emission peak intensities are quantified to calculate the asymmetry ratio (R), which is the peak intensity ratio of the electric dipole (ED) to the magnetic dipole (MD) transition of Tb³⁺ and Eu³⁺ (see Table 1).

2.5. X-ray Photoelectron Spectroscopy (XPS). XPS measurements were performed on a Scienta Omicron ESCA 2SR XPS system equipped with a monochromatic Al K α (hv-1486.6eV) x-ray source and a hemispherical analyzer with a 128-channel detector. The inherent Gaussian width of the photon source was 0.2 eV and the pressure inside the chamber was maintained at 1.5×10^{-9} Torr. The XPS spectra were calibrated to adventitious C 1s peak at 284.6 eV. Peak quantification was performed using Voigt function (70% Gaussian and 30% Lorentzian) in CasaXPS software⁴⁴ after subtracting the Shirley background.

2.6. X-Ray Absorption Spectroscopy (XAS). The local electronic structure was probed via soft-XAS. O K edge and Ce M edge spectra were collected at varied line space plane grating monochromator (VLSPGM: 0.2-1.2 keV) beam line.⁴⁵ The samples were prepared on a carbon tape and were placed inside vacuum chamber using a load-lock. Total electron yield (TEY) detection mode with higher grating and 100 μm slit width was used for these low energy XAS measurements. The obtained XANES data is analyzed using Athena software.⁴⁶

3. Results and Discussion

YZO:Tb, Ce NPs were synthesized via a two-step co-precipitation/molten salt procedure using an equimolar Y to Zr precursor ratio, 2 mol% Tb, and varying Ce concentrations (0, 0.5, 2, and 10 mol%). $^{42-43}$ All the diffraction peaks shown in the XRD pattern of YZO:Tb, Ce NPs (Figure 1(a)) are indexed to the cubic Y₂Zr₂O₇ (ICDD 81-8080, space group *Fm-3m*), which prove the absence of any impurity phases in the as-synthesized NPs. Furthermore, a lattice parameter of 5.20 Å was calculated (Bragg's law), and slightly increased with Ce doping due to the ionic radii of the cations (Tb⁴⁺ < Ce⁴⁺ < Y³⁺ < Tb³⁺ < Ce³⁺). $^{47-53}$ The increasing lattice parameters with doping agree with the effective ionic radii of metal ions. To further determine the local structure

and ensure the formation of the desired disordered fluorite phase, Raman spectroscopy was performed (Figure 1(b)). For the as-synthesized YZO:Tb, Ce NPs, a clear cubic fluorite structure is observed based on the appearance of the T_{2g} peak located near 665 cm⁻¹ for all doping conditions.⁵⁴ Moreover, a red-shift is observed in the peak position with increasing Tb and Ce concentration (Figure 1(b) and S1), which is indicative of an increase in the RE-O bond length. This is consistent with the results of XRD which shows a slight expansion in the lattice parameter upon doping. Additionally, to further confirm the crystallinity of the YZO NPs and identify the crystallite size, HRTEM images were taken. Figure 1(c) shows that the YZO NPs are spherical with ~10 nm diameter with a calculated *d*-spacing of 3.00 Å ((111) lattice plane), which agrees with the cubic $Y_2Zr_2O_7$ structure (ICDD 81-8080). The HRTEM image shows that the as-synthesized NPs have crystallized in single phase without the formation of impurity phases such as ZrO_2 nanoclusters. Overall, the structural characterization shows that the Tb, Ce doping influences the lattice parameters and RE-O bond length of the disordered fluorite $Y_2Zr_2O_7$ NPs, which is especially critical for local symmetry and photoluminescence.

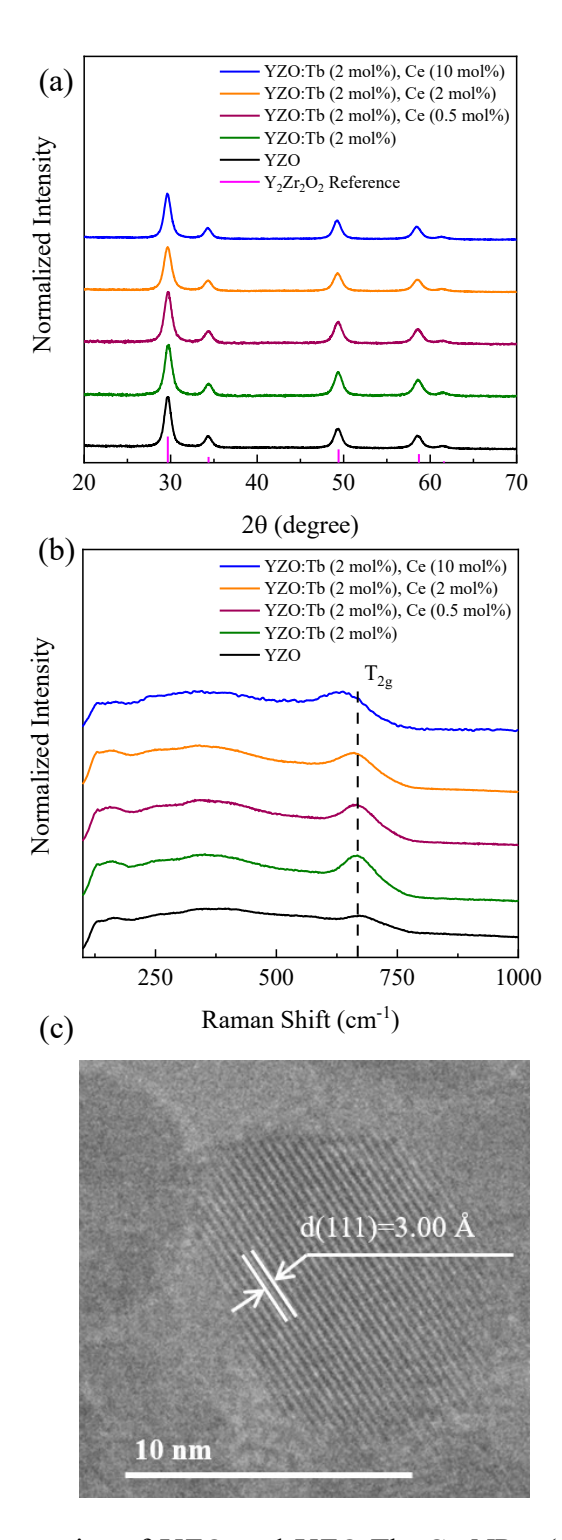


Figure 1. Structural properties of YZO and YZO:Tb, Ce NPs: (a) XRD patterns of assynthesized samples and $Y_2Zr_2O_7$ stoichiometric reference (ICDD 81-8080, space group Fm-3m), which indicates the 2-step synthesis method can create a homogeneous cubic structure and these sample match the stoichiometry of Y:Zr:O=2:2:7. (b) Raman spectra which indicates the as-synthesized samples have cubic fluorite structure and do not change with dopant concentration. (c) HR-TEM of YZO shows a lattice parameter of ~3Å which agrees with the d spacing calculated from XRD.

To investigate the luminescent behavior of the as-synthesized YZO:Tb, Ce NPs, PL spectroscopy was performed. Figure 2(a) shows the PL excitation and emission spectra of YZO:Tb NPs with increasing Tb concentration (2-12.5 mol%). The broad excitation band centered at 258 nm is related to the Tb 4*f*-5*d* transition. The 4*f*-4*f* excitations were not detected in these measurements as they are outside of the excitation filter window (250~380 nm) and the weak intensity of those forbidden transitions. Upon 258 nm excitation, the characteristic $Tb^{3+5}D_{4}-^{7}F_{J}$ (J = 3-6) radiative transitions are observed. The emission intensity of these Tb³⁺ peaks is self-quenched with increasing concentration, as is reported with smaller NPs,55 with 2

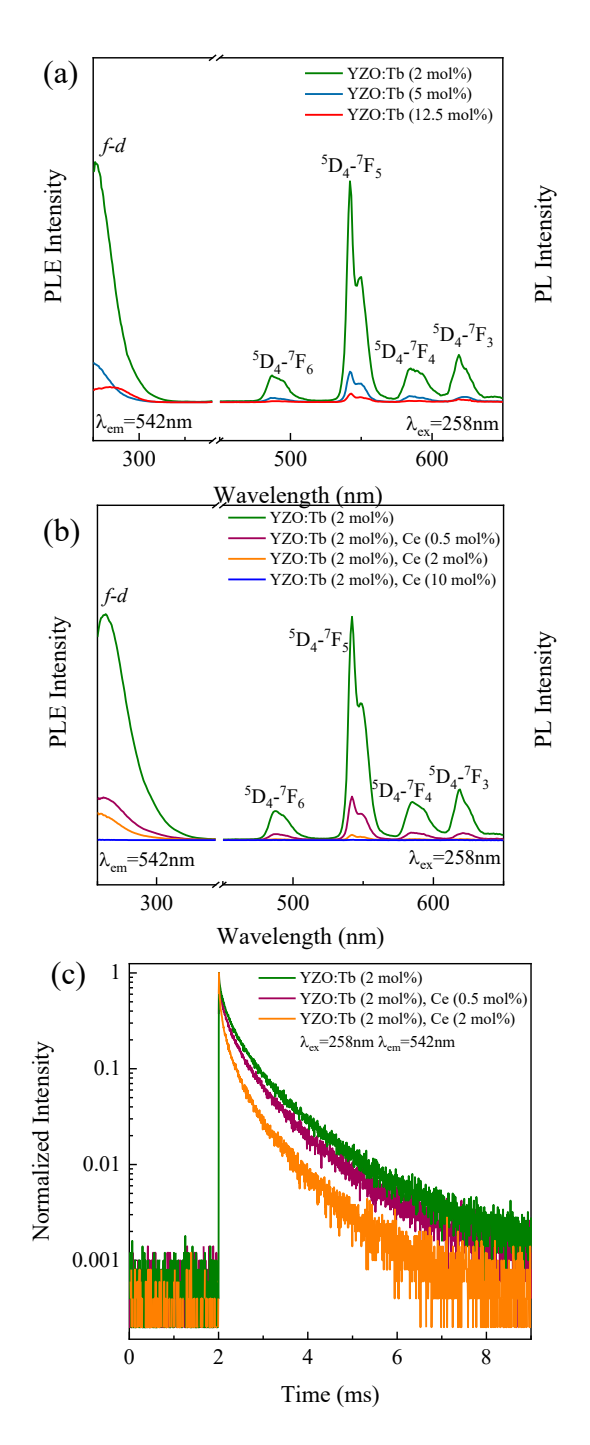


Figure 2. PL measurement of YZO:Tb, Ce NPs: (a) PL spectra of YZO:Tb which show that emission intensity decreases with increasing Tb concentration. (b) PL spectra of YZO:Tb, Ce show reduced intensity with increasing Ce concentration. The emission spectra were excited at λ_{ex} =258 nm. (c) Decay curves of YZO: Tb, Ce at λ_{em} =542 nm emission and λ_{ex} =258 nm excitation.

mol% having the highest emission intensity. Due to this fact, YZO:Tb (2 mol%) was chosen as the reference system for subsequent doping. Opposite of expectations, a systematic decrease in the luminescence intensity is observed after introducing Ce into the YZO:Tb (2 mol%) system (Figure 2(b)). Even with low Ce co-doping (0.5 mol%), the intensity of the 5D_4 - 7F_5 (542 nm) transition peak is quenched by 80%, with further quenching up to 95% at 10 mol% Ce co-doping (Figure S2, Supporting Information). This phenomenon of luminescence quenching with Ce doping was corroborated from the lifetimes of the 5D_4 - 7F_5 transition in YZO:Tb, Ce co-doped NPs and comparable to a Y₂O₃ reference (Table 1). 56 The Tb³⁺ lifetimes were extracted using a second order exponential decay function and showed a decreasing trend with increasing Ce concentration (Figure 2(c)). Introducing up to 2 mol% Ce into the YZO:Tb (2 mol%) system decreases the Tb lifetime, indicating no effective energy transfer from Ce to Tb. 57 The lifetime of YZO:Tb (2 mol%), Ce (10 mol%) was not measured due to its extremely low emission intensity. Therefore, these results show that introducing Ce into YZO:Tb system reduces the Tb³⁺ emission intensity, contrary to the expected Ce sensitization phenomenon. ${}^{33-34,58}$

Table 1. PL lifetimes of the Tb³⁺ $^5D_{4^-}$ 7F₅ (542 nm) and Eu³⁺ $^5D_{0^-}$ 7F₂ (608 nm) transitions of doped YZO:Tb/Eu³⁺, Ce NPs. Tb³⁺ doped Y₂O₃⁵⁶ and Eu³⁺ doped La₂Zr₂O₇⁶¹ are included as references. The asymmetry ratio (R) was calculated from the Eu³⁺ I_{ED}(607 nm)/I_{MD}(590 nm) and Tb³⁺ I_{ED}(542 nm)/I_{MD}(488 nm) transitions.

	$\tau_1(\mu s)$	$\tau_2(\mu s)$	R
Y ₂ O ₃ :Tb ³⁺	130	780	-
YZO:Tb (2 mol%)	273	911	7.69
YZO:Tb (2 mol%), Ce (0.5 mol%)	246	840	7.14
YZO:Tb (2 mol%), Ce (2 mol%)	234	776	5.56
YZO:Tb (2 mol%), Ce (10 mol%)	-	-	2.78
$\text{La}_2\text{Zr}_2\text{O}_7\text{:Eu}^{3+}$	1930		-
YZO:Eu ³⁺ (2 mol%)	1320	-	2.82
YZO:Eu ³⁺ (2 mol%), Ce (0.5 mol%)	1536	-	2.73
YZO:Eu ³⁺ (2 mol%), Ce (2 mol%)	1577	-	2.61
YZO:Eu ³⁺ (2 mol%), Ce (10 mol%)	-	-	2.56

Two mechanisms for this quenching are believed to be possible, the quenching due to changes in local crystal symmetry or due to changes in the oxidation state of Tb. According to previous reports,³⁸ the local symmetry of the RE ion significantly impacts the resultant photoluminescence. In the case that the luminescent ion occupies a more symmetric site, the fluorescence intensity is reduced due to the vibrational relaxation of RE-O bonds.³⁸ As previously discussed, Eu³⁺ is used as a symmetry probe due to the ED transition which is sensitive to the local symmetry around the luminescence center site and does not change oxidation state. Therefore, to understand the changes in the symmetry induced upon Ce doping, Eu³⁺ was introduced as a

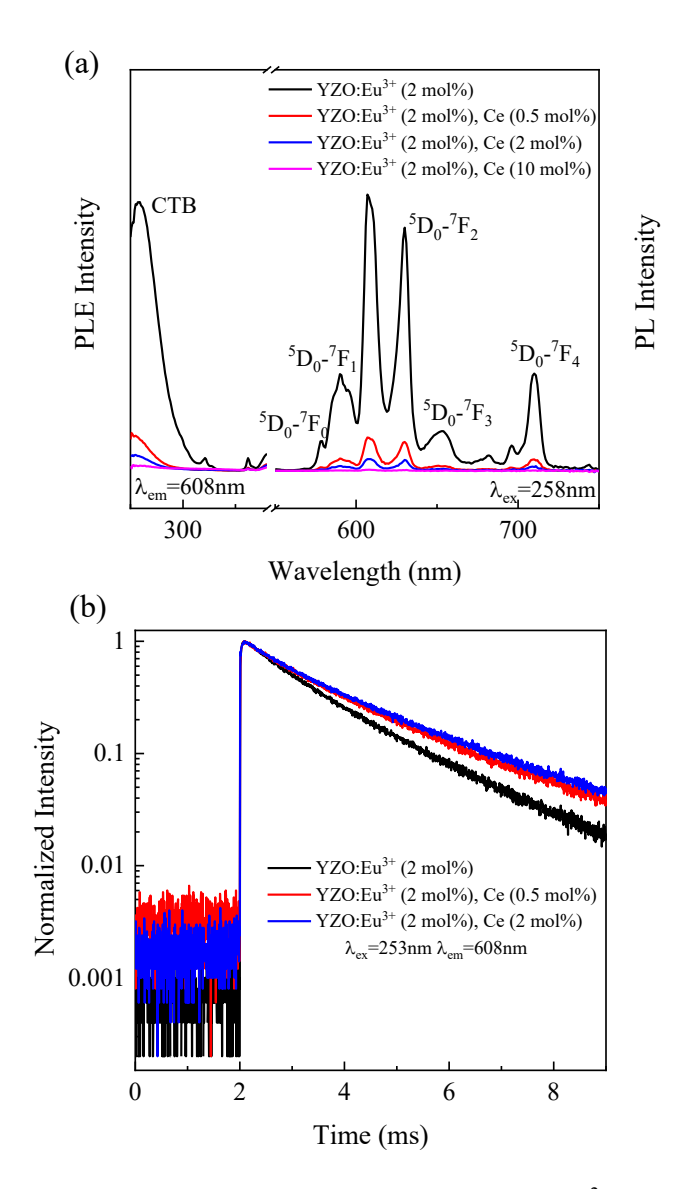


Figure 3. (a) PL measurement of YZO:Eu³⁺, Ce NPs: PL spectra of YZO:Eu³⁺, Ce shows that Ce dopant also quenches Eu³⁺ emission significantly. The emission spectra were measured by exciting with the charge transfer band (CTB, λ_{ex} =258 nm). (b) Decay curves of YZO: Eu³⁺, Ce with λ_{em} =608 nm emission and λ_{ex} =258 nm excitation.

luminescent probe into the crystal due to its symmetry-dependent transitions. ⁵⁹ The Eu³⁺ asymmetry ratio (R) has been used as a probe to determine the local environment around Eu³⁺ in

the YZO lattice. Figure 3(a) shows the emission and excitation spectra of YZO:Eu³⁺ (2 mol%), Ce (0-10 mol%) with the main excitation and emission peaks labelled.⁶⁰ The calculated asymmetry ratios of YZO:Eu³⁺, Ce NPs are shown in Table 1 which is based on the intensity ratio of ED (⁵D₀-⁷F₂ transition, 607 nm) to MD (⁵D₀-⁷F₁ transition, 590 nm). The *R* ratio decreases with increasing Ce concentration, suggesting there is higher local crystal symmetry with Ce incorporation (Table 1). This high symmetry further proves that the oxygen vacancy concentration is decreasing and thereby, transforms the disordered fluorite (low symmetry) a more ordered fluorite phase. Meanwhile, the Eu³⁺ lifetime was also measured (Figure 3(b)). The decay curve shows an increasing lifetime with higher Ce doping and is attributed to the symmetry dependent breakdown in the parity selection rules. The Eu³⁺ emission lifetimes were extracted with a single exponential decay and the results are comparable with the those reported for a La₂Zr₂O₇ host.⁶¹

Similarly, an *R* ratio can also be defined for the Tb³⁺ system using the ED and MD transitions. In this case, the ratio would be the intensities of the ⁵D₄-⁷F₅ transition band (542 nm, ED transition) and the ⁵D₄-⁷F₆ transition band (488 nm, MD transition).⁶² Taking the *R* ratio for the YZO:Tb, Ce samples resulted in a similar trend as with the Eu³⁺ doped materials (Table 1). Additionally, the YZO:Tb (2 mol%) was annealed at 800 °C for 6 h to study the effect of annealing (i.e., oxygen incorporation) on the luminescence performance and lifetime. Both the intensity (Figure S3(a)) and lifetime (Figure S3 (b) and Table S1) decreased after annealing. For comparison, the lifetime of YZO:Tb (5 mol%, Figure S3(b)) was also measured to separate Tb oxidation from self-quenching. Interestingly, the luminescent lifetime of the self-quenching mechanism (YZO:Tb (5 mol%)) has a shorter lifetime than the co-doped sample. Based on this trend, the lifetime measurements suggesting the annealing process increases intraparticle energy transfer and

surface quenching as opposed to oxidation. Furthermore, the Tb³⁺ *R* ratio does not change upon annealing indicting energy transfer is the sole quenching mechanism. Effectively, both the Eu³⁺ and Tb³⁺ asymmetry ratios in the YZO:Tb/Eu³⁺, Ce NPs indicate that the Ce doping increases the symmetry around the luminescent centers, which leads to a higher possibility of vibrational relaxation and therefore, contributes to the observed reduction in the fluorescence intensity.

Next, to determine the oxidation state of RE dopants and quantify the oxygen vacancy concentration, XPS and XANES were performed on the YZO:Tb, Ce NPs. The Y 3*d* peak was deconvoluted into two different doublet peaks corresponding to the Y 3*d*_{5/2} and Y 3*d*_{3/2} peaks (Figure 4(a)). The doublet at 156.0 eV and 158.1 eV can be attributed to Y³⁺ ions. Furthermore, the sharp peak located at 149.2 eV, corresponds to Tb 4*d* of Tb³⁺ ion.⁶³ However, after introducing Ce into this system, i.e. in YZO:Tb (2 mol%), Ce (2 mol%), the Tb 4*d* peak at 149.2 eV disappears and another peak (157.7 eV) appears within the Y 3*d* peak, corresponding to the presence of Tb⁴⁺ ions.⁶⁴⁻⁶⁵ The fact that the YZO:Tb (2 mol%), Ce (2 mol%) still results in emission suggests that Tb³⁺ is still present in the sample; however, lack of a Tb³⁺ signature in the

XPS can be attributed to the concentration being below the instrument detection limit. Therefore, the change in Tb 4d peak reveals that the incorporation of Ce into the YZO host drives the Tb³⁺ to the non-luminescent Tb⁴⁺ state, reducing the luminescent centers in the host. On the other hand, Zr 3d spectra show two different species of Zr (Zr⁴⁺ and reduced Zr ions) in the doped YZO NPs (Figure 4(b)). The Zr 3d peaks were also deconvoluted into two doublet peaks. The doublet peaks at 180.9 eV (Zr $3d_{5/2}$) and 183.3 eV (Zr $3d_{3/2}$) correspond to Zr⁴⁺, and the doublet at 178.9 eV and 181.4 eV indicate the presence of reduced Zr ions.⁶⁶ To corroborate the reduction in the oxygen vacancies with increasing Ce concentration as observed from the PL spectra, the O 1s detailed spectra was collected (Figure 4(c)). The main O 1s peak centered at \sim 529 eV is attributed to the lattice O²- ion, a weak peak centered at ~530 eV is due to the O-H surface groups, and a peak at ~532 eV is

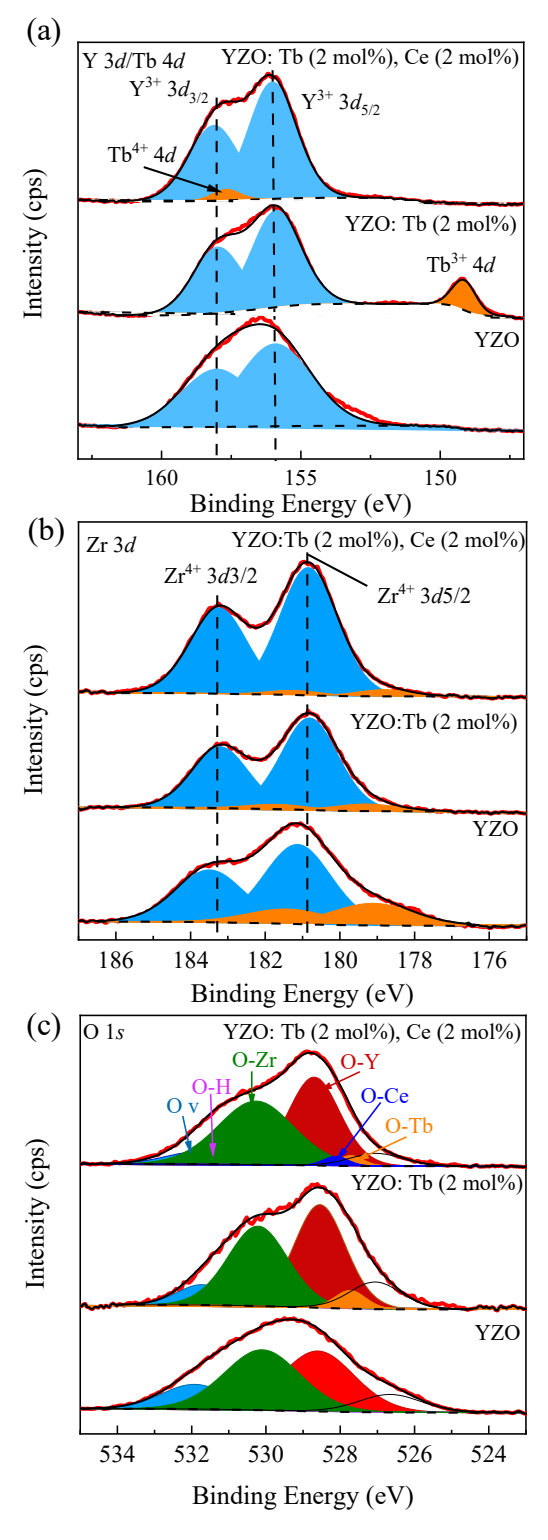


Figure 4. Deconvoluted XPS spectra for the different YZO:Tb, Ce NPs compositions. (a) Y 3d/Tb 4d (b) Zr 3d and (c) O 1s peaks.

ascribed to the under coordinated cations or oxygen vacancies.⁶⁷ The area under the oxygen vacancy peak is observed to decrease with Ce doping, which agrees with the decreasing trend of the reduced Zr ion peaks in Zr 3d spectra and the oxidization of Tb³⁺ to Tb⁴⁺, as well as the higher symmetry from the asymmetry ratios of Eu³⁺ and Tb³⁺.

Owing to the lower concentrations of Ce, the oxidation state of Ce was quantified using the Ce M edge XANES spectra due to higher sensitivity than XPS at these concentrations. The Ce oxidation state in YZO:Tb (2 mol%), Ce (x mol%) (x=0.5, 2, 10) samples was determined to be 4+ based on the standard CeO₂ (Figure 5).⁶⁸ The O K edge XANES were also measured (Figure S4, Supporting Information). The hybridization peaks are identified in Table S2 (Supporting Information). Since the O 2p orbitals hybridize with the cation (Y³⁺, Zr⁴⁺, Tb^{3+/4+}, Ce^{3+/4+}) d orbitals,⁶⁹ it was difficult to decipher the distribution of oxygen vacancies from the O K edge XANES spectra. However, by comparing the doped samples O K edge with the CeO₂ reference, a peak begins to form for higher (≥ 2 mol%) Ce doping concentrations at 529.7 eV (labeled (a))

and matches well to the reference.⁷⁰ Coupling this with the previous results indicating that the Ce⁴⁺ oxidation state begins to be prominent at higher concentrations but plays a role in all samples.

Overall, the XPS and XANES results indicate that the Ce is in 4+ oxidation state in the YZO:Tb, Ce

NPs, resulting in the oxidation of Tb from 3+ to 4+ and removes excess oxygen vacancies within the crystals.

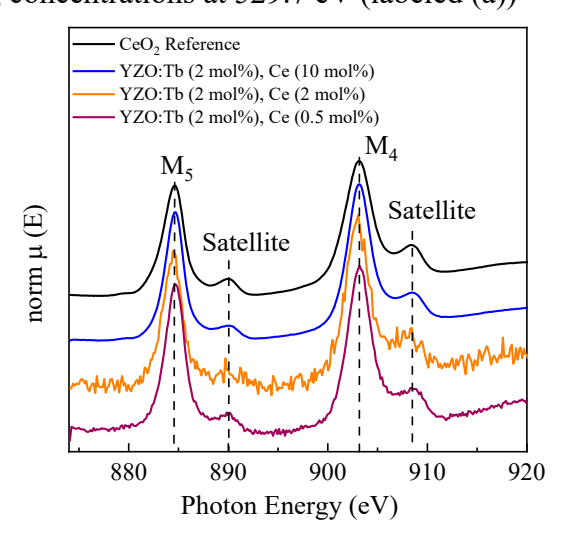


Figure 5. XANES Ce M Edge of YZO:Tb, Ce NPs: Ce M₅ (884.6 eV) and M₄ (903.0 eV) edge of the samples containing Ce and CeO₂ reference. The satellite peaks located at 890 eV and 908.4 eV are characteristic to Ce⁴⁺.

From the results of PL, XPS, and XANES, it can be concluded that the YZO:Tb has the typical Tb³⁺ emission, which disappears after introducing Ce due to the oxidation of Tb³⁺ to Tb⁴⁺. The PL spectra of the YZO:Eu³⁺, Ce reveals that the Ce incorporation in the host changes the local structure surrounding luminescence center, reducing the degree of disorder in the YZO:Tb, Ce NPs. Furthermore, XPS spectra of Zr 3d suggests that Ce and Tb dopants oxidize the reduced Zr ions. Additionally, the O 1s XPS spectra shows decreasing concentration of oxygen vacancy with increasing Ce doping. As shown in Figure 6(a) and (b), incorporation of Ce as Ce⁴⁺ fully oxidizes the other cations (Y, Zr and Tb) through the incorporation of more oxygen ions into the lattice resulting in a more symmetric structure (ordered fluorite). This higher level of local symmetry surrounding the Tb sites increases the possibility of vibrational relaxation, and thereby reduces the fluorescence intensity. Figure 6(c) shows the energy diagram of the sensitizer pair of Ce³⁺-Tb³⁺, the sensitizing effect is mainly created by the broad absorption cross section of Ce³⁺ from ground state to 5d level. In the case of this work, Ce exists as Ce⁴⁺ in YZO host, which does not have electron transfer to 5d level. As a result, there is no energy transfer exist in YZO:Ce, Tb NPs. In addition, the luminescence is further inhibited by the oxidation of the Tb from 3+ to 4+ state.

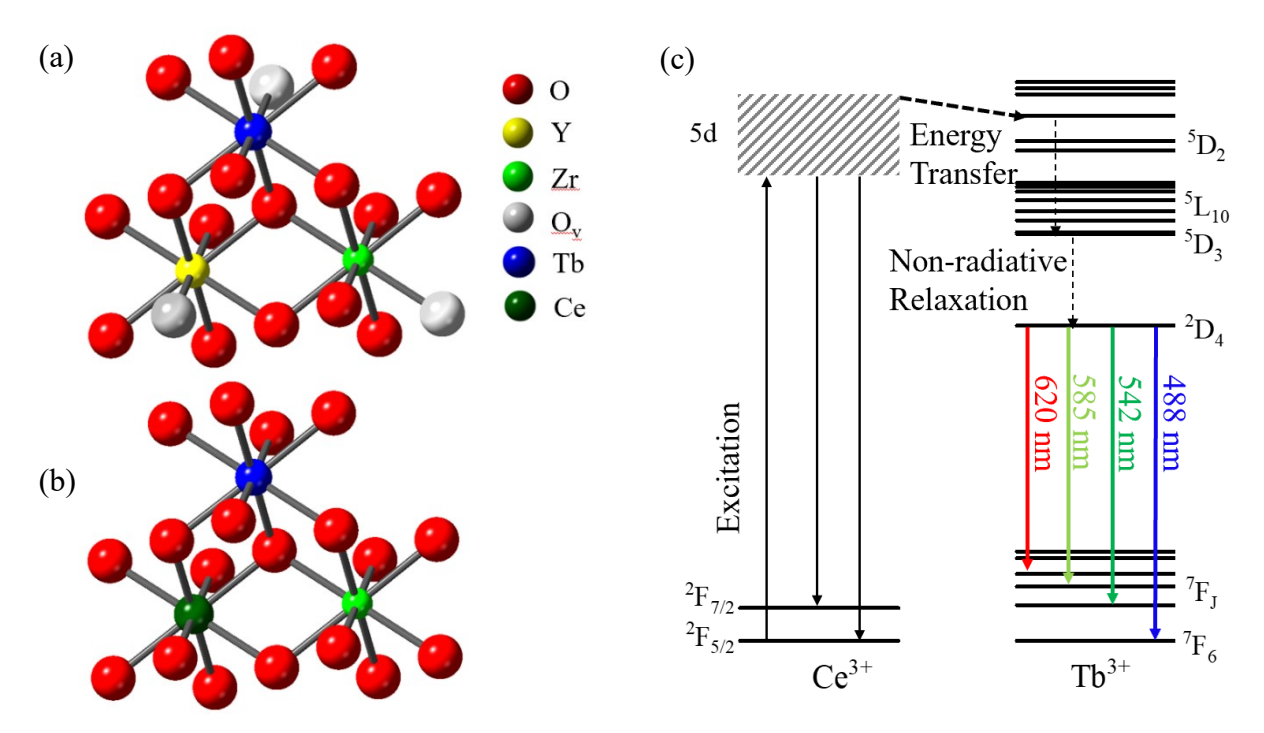


Figure 6. (a) Local structure of YZO:Tb NPs with oxygen vacancies (grey balls) randomly occupying anion sites. (b) After introducing Ce (olive green ball) into NPs, the oxygen vacancies surrounding the luminescence center (Tb, blue ball) are filled with oxygen atoms (red balls), furthermore, improve the symmetry level of the local environment surrounding Tb. (c) Energy level diagram of the sensitizer pair Ce³⁺-Tb³⁺ highlighting radiative and non-radiative processes.

4. Summary

In summary, YZO:Tb, Ce and YZO:Eu³⁺, Ce NPs were synthesized using a two-step coprecipitation and molten salt synthesis method. XPS, Raman and HRTEM show that the as synthesized RE doped YZO samples crystallized into a cubic disordered fluorite phase. The emission and excitation intensity of Tb in YZO host was quenched after introducing Ce, which is contrary to the expected Ce sensitization effect. This anomaly is explained from both the change in the local symmetry and oxidation state of the luminescent center. First, introducing Ce into the YZO:Tb samples increases the local symmetry surrounding the luminescent centers (Tb), which is probed using the transitions of the Eu³⁺ that are sensitive to local symmetry. Furthermore, XPS and XANES spectra show that Ce⁴⁺ drives the Tb³⁺ to Tb⁴⁺, reducing the concentration of

luminescent centers. Ultimately, this work demonstrates that host materials can result in quenching with common sensitization ions and careful selection of the materials is needed to ensure high intensity luminescence for phosphors.

ASSOCIATED CONTENT

Supporting Information.

The Supporting Information is available free of charge on the ACS Publications website at DOI: PL emission intensity quenching relationship diagram, PL decay lifetime, XANES O K edge.

AUTHOR INFORMATION

Corresponding Author

*Email: jamesdorman@lsu.edu

Author Contributions

Y.W. has performed the synthesis of YZO:Tb/Eu, Ce NPs and completed the XRD, Raman, HRTEM, XPS analysis. P.D. has assisted XPS measurement and analysis. O.K. has performed

XANES measurements and assisted XANES analysis. Y.W. and J.A.D. have planned and contributed to the writing of the manuscript.

Funding Sources

Y.W. and J.A.D. acknowledge the National Science Foundation Macromolecular, Supramolecular, and Nanochemistry directorate (CHE-1709902). Supplies and characterization were funded by the Louisiana Board of Regents (LEQSF(2016-19)-RD-A-03).

ACKNOWLEDGMENT

Y.W. acknowledges Tochukwu Ofoegbuna for performing XRD measurements, Behnam Safavinia for performing Raman measurements and Natalia Moura for the HRTEM measurements.

REFERENCES

- 1. Li, Y.; Kowalski, P. M.; Beridze, G.; Birnie, A. R.; Finkeldei, S.; Bosbach, D., Defect Formation Energies in A₂B₂O₇ Pyrochlores. *Scr. Mater.* **2015**, *107*, 18-21.
- 2. Scheetz, B. E.; White, W. B., Characterization of Anion Disorder in Zirconate A₂B₂O₇ Compounds by Raman Spectroscopy. *J. Am. Ceram. Soc.* **1979**, *62*, 468-470.
- 3. Pirzada, M.; Grimes, R. W.; Minervini, L.; Maguire, J. F.; Sickafus, K. E., Oxygen Migration in A₂B₂O₇ Pyrochlores. *Solid State Ion.* **2001**, *140*, 201-208.
- 4. Jovaní, M.; Beltrán-Mir, H. c.; Cordoncillo, E.; West, A. R., Atmosphere-and Voltage-Dependent Electronic Conductivity of Oxide-Ion-Conducting Zr_{1-X}Y_xO_{2-X/2} Ceramics. *Inorg. Chem.* **2017**, *56*, 7081-7088.
- 5. Zhang, X.; Fang, X.; Feng, X.; Li, X.; Liu, W.; Xu, X.; Zhang, N.; Gao, Z.; Wang, X.; Zhou, W., Ni/ Ln₂Zr₂O₇ (Ln= La, Pr, Sm and Y) Catalysts for Methane Steam Reforming: The Effects of a Site Replacement. *Catal. Sci. Technol.* **2017**, *7*, 2729-2743.

- 6. Ma, Y.; Wang, X.; You, X.; Liu, J.; Tian, J.; Xu, X.; Peng, H.; Liu, W.; Li, C.; Zhou, W., Nickel-Supported on La₂Sn₂O₇ and La₂Zr₂O₇ Pyrochlores for Methane Steam Reforming: Insight into the Difference between Tin and Zirconium in the B Site of the Compound. *ChemCatChem* **2014**, *6*, 3366-3376.
- 7. Jovani, M.; Sanz, A.; Beltran-Mir, H.; Cordoncillo, E., New Red-Shade Environmental-Friendly Multifunctional Pigment Based on Tb and Fe Doped Y₂Zr₂O₇ for Ceramic Applications and Cool Roof Coatings. *Dyes Pigments* **2016**, *133*, 33-40.
- 8. Weber, S. B.; Lein, H. L.; Grande, T.; Einarsrud, M.-A., Lanthanum Zirconate Thermal Barrier Coatings Deposited by Spray Pyrolysis. *Surf. Coat. Tech.* **2013**, *227*, 10-14.
- 9. Nyman, M.; Rodriguez, M. A.; Shea-Rohwer, L. E.; Martin, J. E.; Provencio, P. P., Highly Versatile Rare Earth Tantalate Pyrochlore Nanophosphors. *J. Am. Chem. Soc.* **2009**, *131*, 11652-11653.
- 10. Fujihara, S.; Tokumo, K., Multiband Orange-Red Luminescence of Eu³⁺ Ions Based on the Pyrochlore-Structured Host Crystal. *Chem. Mater.* **2005**, *17*, 5587-5593.
- 11. Zeng, J.; Wang, H.; Zhang, Y.; Zhu, M. K.; Yan, H., Hydrothermal Synthesis and Photocatalytic Properties of Pyrochlore La₂Sn₂O₇ Nanocubes. *J. Phys. Chem. C* **2007**, *111*, 11879-11887.
- 12. Otaki, H.; Kido, H.; Hoshikawa, T.; Shimada, M.; Koizumi, M., Crystal Structure and Fluorescence Properties of R₂Zr₂O₇ and (R_{1-x}Eu_x)₂Zr₂O₇ Compounds. *J. Ceram. Soc. Jpn.* **1988**, *96*, 124-126.
- 13. Zhang, A.; Lü, M.; Yang, Z.; Zhou, G.; Zhou, Y., Systematic Research on Re₂Zr₂O₇ (Re=La, Nd, Eu and Y) Nanocrystals: Preparation, Structure and Photoluminescence Characterization. *Solid State Sci.* **2008**, *10*, 74-81.
- 14. Subramanian, M. A.; Aravamudan, G.; Subba Rao, G. V., Oxide Pyrochlores a Review. *Prog. Solid State Ch.* **1983**, *15*, 55-143.
- 15. Abarghooei, M. A.; Mohebat, R.; Karimi-Jaberi, Z.; Mosslemin, M. H., An Efficient Synthesis of Naphtho 2,1-B Furan-2(1h)-Ones Catalysed by Nafion-H Supported on Silica-Coated Super Paramagnetic Iron Oxide Nanoparticles. *J. Chem. Res.* **2017**, 408-412.
- 16. Gilardi, E.; Gregori, G.; Wang, Y.; Sigle, W.; van Aken, P. A.; Maier, J., Interface Effects on the Ion Transport of Epitaxial Y₂Zr₂O₇ Films. *ACS Appl. Mater. Interfaces* **2017**, *9*, 27257-27265.
- 17. Aschauer, U.; Pfenninger, R.; Selbach, S. M.; Grande, T.; Spaldin, N. A., Strain-Controlled Oxygen Vacancy Formation and Ordering in Camno 3. *Phys. Rev. B* **2013**, *88*, 054111.

- 18. Wang, J.; Liu, P.; Fu, X.; Li, Z.; Han, W.; Wang, X., Relationship between Oxygen Defects and the Photocatalytic Property of Zno Nanocrystals in Nafion Membranes. *Langmuir* **2009**, *25*, 1218-1223.
- 19. Yahiro, H.; Eguchi, K.; Arai, H., Electrical Properties and Reducibilities of Ceria-Rare Earth Oxide Systems and Their Application to Solid Oxide Fuel Cell. *Solid State Ion.* **1989**, *36*, 71-75.
- 20. Darapaneni, P.; Moura, N. S.; Harry, D.; Cullen, D. A.; Dooley, K. M.; Dorman, J. A., Effect of Moisture on Dopant Segregation in Solid Hosts. *J. Phys. Chem. C* **2019**, *123*, 12234-12241.
- 21. Zhang, A.; Lü, M.; Qiu, Z.; Zhou, Y.; Ma, Q., Multiband Luminescence of Eu³⁺ Based on Y₂Zr₂O₇ Nanocrystals. *Mater. Chem. Phys.* **2008**, *109*, 105-108.
- 22. Du, Q.; Zhou, G.; Zhou, J.; Jia, X.; Zhou, H., Enhanced Luminescence of Novel Y₂Zr₂O₇:Dy³⁺ Phosphors by Li⁺ Co-Doping. *J. Alloys Comd.* **2013**, *552*, 152-156.
- 23. Du, Q.; Zhou, G.; Zhou, H.; Yang, Z., Novel Multiband Luminescence of Y₂Zr₂O₇: Eu³⁺, R³⁺ (R= Ce, Bi) Orange–Red Phosphors Via a Sol–Gel Combustion Approach. *Opt. Mater.* **2012**, *35*, 257-262.
- 24. Gao, L.; An, Y.; Zhu, H.; Wang, L.; Chen, J.; Wang, N.; Ou, G., Hydrothermal Synthesis and Photoluminescence Properties of Y₂Zr₂O₇: Tb³⁺ Phosphors. *J. Mater. Sci.* **2011**, *46*, 1337-1340.
- 25. Xia, Z.; Liu, R.-S., Tunable Blue-Green Color Emission and Energy Transfer of Ca₂Al₃O₆F:Ce³⁺,Tb³⁺ Phosphors for near-Uv White Leds. *J. Phys. Chem. C* **2012**, *116*, 15604-15609.
- 26. Shaat, S. K. K.; Swart, H. C.; Ntwaeaborwa, O. M., Tunable and White Photoluminescence from Tb³⁺–Eu³⁺ Activated Ca_{0.3}Sr_{0.7}Al₂O₄ Phosphors and Analysis of Chemical States by X-Ray Photoelectron Spectroscopy. *J. Alloys Comd.* **2014**, *587*, 600-605.
- 27. Vaithiyanathan, M.; R. Bajgiran, K.; Darapaneni, P.; Safa, N.; Dorman, J. A.; Melvin, A. T., Luminescent Nanomaterials for Droplet Tracking in a Microfluidic Trapping Array. *Anal. Bioanal. Chem.* **2019**, *411*, 157-170.
- 28. Chen, J.; Guo, H.; Li, Z.; Zhang, H.; Zhuang, Y., Near-Infrared Quantum Cutting in Ce³⁺, Yb³⁺ Co-Doped YBO₃ Phosphors by Cooperative Energy Transfer. *Opt. Mater.* **2010**, *32*, 998-1001.
- 29. Chen, M.; Xia, Z.; Liu, Q., Luminescence Properties and Energy Transfer of Ce³⁺/Tb³⁺ Co-Doped Ca₆Ba(PO₄)₄O Phosphor for near-UV Pumped Light-Emitting Diodes. *J. Mater. Chem. C* **2015**, *3*, 4197-4204.

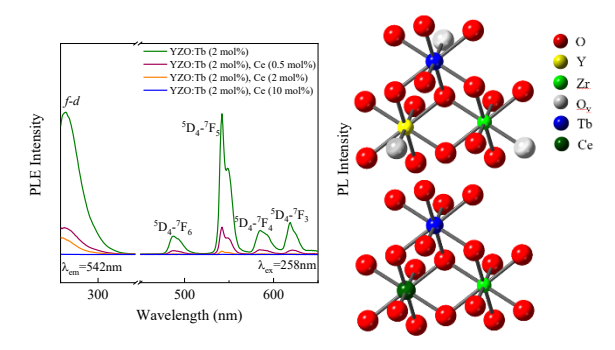
- 30. Wang, W.; Tang, J.; Hsu, S. T.; Wang, J.; Sullivan, B. P., Energy Transfer and Enriched Emission Spectrum in Cr and Ce Co-Doped Y₃Al₅O₁₂ Yellow Phosphors. *Chem. Phys. Lett.* **2008**, *457*, 103-105.
- 31. Xu, J.; Ueda, J.; Kuroishi, K.; Tanabe, S., Fabrication of Ce³⁺–Cr³⁺ Co-Doped Yttrium Aluminium Gallium Garnet Transparent Ceramic Phosphors with Super Long Persistent Luminescence. *Scr. Mater.* **2015**, *102*, 47-50.
- 32. Zhang, X.; Huang, Y.; Gong, M., Dual-Emitting Ce³⁺, Tb³⁺ Co-Doped Laobr Phosphor: Luminescence, Energy Transfer and Ratiometric Temperature Sensing. *Chem. Engr. J.* **2017**, *307*, 291-299.
- 33. Nigam, S.; Sudarsan, V.; Vatsa, R. K.; Ghattak, J.; Satyam, P., Improved Energy Transfer between Ce³⁺ and Tb³⁺ Ions at the Interface between Y₂Sn₂O₇: Ce³⁺, Tb³⁺ Nanoparticles and Silica. *J. Phys. Chem. C* **2009**, *113*, 8750-8755.
- 34. Lai, H.; Bao, A.; Yang, Y.; Tao, Y.; Yang, H.; Zhang, Y.; Han, L., UV Luminescence Property of YPO₄:Re (Re = Ce³⁺, Tb³⁺). *J. Phys. Chem. C* **2008**, *112*, 282-286.
- 35. Dorman, J. A.; Choi, J. H.; Kuzmanich, G.; Chang, J. P., High-Quality White Light Using Core–Shell Re³⁺:LaPO₄ (Re = Eu, Tb, Dy, Ce) Phosphors. *J. Phys. Chem. C* **2012**, *116*, 12854-12860.
- 36. Hsu, C.-H.; Lu, C.-H., Microwave-Hydrothermally Synthesized (Sr_{1-X-Y} Ce_X Tb_Y) $Si_2O_{2-\delta}N_{2+\mu}$ Phosphors: Efficient Energy Transfer, Structural Refinement and Photoluminescence Properties. *J. Mater. Chem.* **2011**, *21*, 2932-2939.
- 37. Flores-Gonzalez, M.; Ledoux, G.; Roux, S.; Lebbou, K.; Perriat, P.; Tillement, O., Preparing Nanometer Scaled Tb-Doped Y₂O₃ Luminescent Powders by the Polyol Method. *J. Solid State Chem.* **2005**, *178*, 989-997.
- 38. Kumar, A.; Babu, S.; Karakoti, A. S.; Schulte, A.; Seal, S., Luminescence Properties of Europium-Doped Cerium Oxide Nanoparticles: Role of Vacancy and Oxidation States. *Langmuir* **2009**, *25*, 10998-11007.
- 39. Goodenough, J. B., Ceramic Technology: Oxide-Ion Conductors by Design. *Nature* **2000**, *404*, 821.
- 40. Wang, J.; Wang, Z.; Huang, B.; Ma, Y.; Liu, Y.; Qin, X.; Zhang, X.; Dai, Y., Oxygen Vacancy Induced Band-Gap Narrowing and Enhanced Visible Light Photocatalytic Activity of ZnO. *ACS Appl. Mater Interfaces* **2012**, *4*, 4024-4030.
- 41. Li, Y.; Meng, G.; Zhang, L.; Phillipp, F., Ordered Semiconductor ZnO Nanowire Arrays and Their Photoluminescence Properties. *Appl. Phys. Lett.* **2000**, *76*, 2011-2013.
- 42. Mao, Y.; Guo, X.; Huang, J. Y.; Wang, K. L.; Chang, J. P., Luminescent Nanocrystals with A₂B₂O₇ Composition Synthesized by a Kinetically Modified Molten Salt Method. *J. Phys. Chem. C* **2009**, *113*, 1204-1208.

- 43. Ofoegbuna, T.; Darapaneni, P.; Sahu, S.; Plaisance, C.; Dorman, J. A., Stabilizing the B-Site Oxidation State in ABO₃ Perovskite Nanoparticles. *Nanoscale* **2019**, *11*, 14303-14311.
- 44. Fairley, N., *Casaxps Manual 2.3. 15: Casaxpx Processing Software for Xps Spectra*; Casa Software Limited, 2009.
- 45. Morikawa, E.; Ono, M.; Kodukula, S.; Bordelon, A.; Scott, J.; Garber, J.; Perkins, R. In *Infrared Microspectroscopy Beamline at Camd*, AIP Conference Proceedings, AIP: 2004; pp 364-367.
- 46. Ravel, B.; Newville, M., Athena, Artemis, Hephaestus: Data Analysis for X-Ray Absorption Spectroscopy Using Ifeffit. *J. Synchrotron Radiation* **2005**, *12*, 537-541.
- 47. Belver, C.; Bedia, J.; Álvarez-Montero, M.; Rodriguez, J., Solar Photocatalytic Purification of Water with Ce-Doped TiO₂/Clay Heterostructures. *Catal. Today* **2016**, *266*, 36-45.
- 48. Kinoshita, H.; Kuramoto, K. i.; Uno, M.; Yanagi, T.; Yamanaka, S.; Mitamura, H.; Banba, T., Phase Stability of Yttria-Stabilized Zirconia with Dissolved Cerium and Neptunium Oxides under Oxidizing and Reducing Atmospheres. *J. Am. Ceram. Soc.* **2000**, *83*, 391-396.
- 49. Ahrens, L. H., The Use of Ionization Potentials Part 1. Ionic Radii of the Elements. *Geochim. Cosmochim. Acta* **1952**, *2*, 155-169.
- 50. Jia, Y., Crystal Radii and Effective Ionic Radii of the Rare Earth Ions. *J. Solid State Chem.* **1991**, *95*, 184-187.
- 51. Su, Y.-Q.; Liu, J.-X.; Filot, I. A.; Zhang, L.; Hensen, E. J., Highly Active and Stable CH4 Oxidation by Substitution of Ce⁴⁺ by Two Pd²⁺ Ions in CeO₂ (111). *ACS Catal.* **2018**, *8*, 6552-6559.
- 52. Kim, D. J., Lattice Parameters, Ionic Conductivities, and Solubility Limits in Fluorite-Structure MO₂ Oxide [M=Hf⁴⁺, Zr⁴⁺, Ce⁴⁺, Th⁴⁺, U⁴⁺] Solid Solutions. *J. Am. Ceram. Soc.* **1989**, 72, 1415-1421.
- 53. Lu, D.-Y., Self-Adjustable Site Occupations between Ba-Site Tb³⁺ and Ti-Site Tb⁴⁺ Ions in Terbium-Doped Barium Titanate Ceramics. *Solid State Ion.* **2015**, *276*, 98-106.
- 54. Yashima, M.; Ohtake, K.; Kakihana, M.; Arashi, H.; Yoshimura, M., Determination of Tetragonal-Cubic Phase Boundary of Zr_{1-X}R_XO_{2-X/2} (R= Nd, Sm, Y, Er and Yb) by Raman Scattering. *J. Phys. Chem. Solids* **1996**, *57*, 17-24.
- 55. Som, S.; Sharma, S., Eu³⁺/Tb³⁺-Codoped Y₂O₃ Nanophosphors: Rietveld Refinement, Bandgap and Photoluminescence Optimization. *J. Physics D: Appl. Phys.* **2012**, *45*, 415102.
- 56. Stagi, L.; Chiriu, D.; Ardu, A.; Cannas, C.; Carbonaro, C. M.; Ricci, P. C., Luminescence Enhancement by Energy Transfer in Melamine- Y₂O₃: Tb³⁺ Nanohybrids. *J. Appl. Phys.* **2015**, *118*, 125502.

- 57. Yu, H.; Zi, W.; Lan, S.; Gan, S.; Zou, H.; Xu, X.; Hong, G., Green Light Emission by Ce³⁺ and Tb³⁺ Co-Doped Sr₃MgSi₂O₈ Phosphors for Potential Application in Ultraviolet Whitelight-Emitting Diodes. *Opt. Laser Technol.* **2012**, *44*, 2306-2311.
- 58. Guo, N.; Song, Y.; You, H.; Jia, G.; Yang, M.; Liu, K.; Zheng, Y.; Huang, Y.; Zhang, H., Optical Properties and Energy Transfer of NaCaPO₄: Ce³⁺, Tb³⁺ Phosphors for Potential Application in Light-Emitting Diodes. *Eur. J. Inorg. Chem.* **2010**, 2010, 4636-4642.
- 59. Cannas, C.; Casu, M.; Mainas, M.; Musinu, A.; Piccaluga, G.; Polizzi, S.; Speghini, A.; Bettinelli, M., Synthesis, Characterisation and Optical Properties of Nanocrystalline Y₂O₃–Eu³⁺ Dispersed in a Silica Matrix by a Deposition–Precipitation Method. *J. Mater. Chem.* **2003**, *13*, 3079-3084.
- 60. R Bajgiran, K.; Darapaneni, P.; Melvin, A. T.; Dorman, J. A., Effects of Weak Electric Field on the Photoluminescence Behavior of Bi³⁺-Doped YVO₄:Eu³⁺ Core–Shell Nanoparticles. *J. Phys. Chem. C* **2019**, *123*, 13027-13035.
- 61. Pokhrel, M.; Brik, M. G.; Mao, Y., Particle Size and Crystal Phase Dependent Photoluminescence of La₂Zr₂O₇: Eu³⁺ Nanoparticles. *J. Am. Ceram. Soc.* **2015**, *98*, 3192-3201.
- 62. Hong, S. B.; Seo, J. S.; Pyun, C.-H.; Kim, C.-H.; Uh, Y. S., Location of Tb (III) Ions in Na-Y Zeolite Determined by Luminescence Spectroscopy. *Catal. Lett.* **1994**, *30*, 87-97.
- 63. Abualrejal, M. M.; Zou, H.; Chen, J.; Song, Y.; Sheng, Y., Electrospinning Synthesis and Photoluminescence Properties of One-Dimensional SiO₂: Tb+ Nanofibers and Nanobelts. *Adv. Nanopart.* **2017**, *6*, 33.
- 64. Chen, K.; Gao, H.; Bai, B.; Liu, W.; Li, X., Microwave Hydrothermal Synthesis of Terbium Ions Complexed with Porous Graphene for Effective Absorbent for Organic Dye. *Nano. Res. Lett.* **2017**, *12*, 204.
- 65. Masumoto, K.; Semba, A.; Kimura, C.; Taniguchi, T.; Watanabe, K.; Sakata, T.; Aoki, H., Luminescence Characteristics and Annealing Effect of Tb-Doped Albno Films for Inorganic Electroluminescence Devices. *Jpn. J. Appl. Phys.* **2011**, *50*, 04DH01.
- 66. Rahman, M. A.; Rout, S.; Thomas, J. P.; McGillivray, D.; Leung, K. T., Defect-Rich Dopant-Free Zro2 Nanostructures with Superior Dilute Ferromagnetic Semiconductor Properties. *J. Am. Chem. Soc.* **2016**, *138*, 11896-11906.
- 67. Dupin, J.-C.; Gonbeau, D.; Vinatier, P.; Levasseur, A., Systematic XPS Studies of Metal Oxides, Hydroxides and Peroxides. *Phys. Chem. Chem. Phys.* **2000**, *2*, 1319-1324.
- 68. Ranjith, K. S.; Saravanan, P.; Chen, S.-H.; Dong, C.-L.; Chen, C. L.; Chen, S.-Y.; Asokan, K.; Rajendra Kumar, R. T., Enhanced Room-Temperature Ferromagnetism on Co-Doped CeO₂ Nanoparticles: Mechanism and Electronic and Optical Properties. *J. Phys. Chem. C* **2014**, *118*, 27039-27047.

- 69. Darapaneni, P.; Kizilkaya, O.; Wang, Z.; Dorman, J. A., Weak Field Tuning of Transition-Metal Dopant Hybridization in Solid Hosts. *J. Phys. Chem. C* **2018**, *122*, 22699-22708.
- 70. Rodriguez, J. A.; Hanson, J. C.; Kim, J.-Y.; Liu, G.; Iglesias-Juez, A.; Fernández-García, M., Properties of CeO₂ and Ce_{1-X}Zr_XO₂ Nanoparticles: X-Ray Absorption near-Edge Spectroscopy, Density Functional, and Time-Resolved X-Ray Diffraction Studies. *J. Phys. Chem. B* **2003**, *107*, 3535-3543.

For Table of Contents Only



Ce was found to quench Tb^{3+} PL emission intensity in a $Y_2Zr_2O_7$ host. The quenching mechanism was studied to separate oxidation and structural effects on the luminescence centers. These results show that the rare earth dopants are susceptible to the crystal lattice and care must be taken to ensure the system does not significantly change oxidation or structure.